New Journal of Physics
The open access journal at the forefront of physics

Deutsche Physikalische Gesellschaft DPG
IOP Institute of Physics

Published in partnership with: Deutsche Physikalische Gesellschaft and the Institute of Physics

OPEN ACCESS

RECEIVED
15 December 2021

REVISED
12 April 2022

ACCEPTED FOR PUBLICATION
5 May 2022

PUBLISHED
20 May 2022

PAPER

Chaotic dynamics of Bose–Einstein condensate induced by density-dependent gauge field

Lei Chen[1,2] **and Qizhong Zhu**[1,3,*]

[1] Guangdong Provincial Key Laboratory of Quantum Engineering and Quantum Materials, School of Physics and Telecommunication Engineering, South China Normal University, Guangzhou 510006, People's Republic of China
[2] School of Physics and Electronic Science, Zunyi Normal University, Zunyi 563006, People's Republic of China
[3] Guangdong-Hong Kong Joint Laboratory of Quantum Matter, Frontier Research Institute for Physics, South China Normal University, Guangzhou 510006, People's Republic of China
[*] Author to whom any correspondence should be addressed.

E-mail: qzzhu@m.scnu.edu.cn

Keywords: Bose–Einstein condensate, synthetic gauge field, chaotic dynamics

Abstract

In this work we study the effect of density-dependent gauge field on the collective dynamics of a harmonically trapped Bose–Einstein condensate (BEC), beyond the linear response regime. The density-dependent gauge field, as a backaction of the condensate, can in turn affect the condensate dynamics, resulting in highly nonlinear equations of motion. The dipole and breathing oscillations of the condensate along the direction of gauge field are coupled by this field. We find that, in the presence of this coupling, the collective motion of a quasi-one-dimensional condensate is still regular, i.e., periodic or quasiperiodic. In contrast, for a quasi-two-dimensional condensate, the collective dynamics of the condensate can become chaotic, when the density-dependent gauge field is strong. The mechanism is that the gauge field can also induce a Hall effect, manifested as an additional coupling between dipole and breathing oscillations in perpendicular direction, and chaotic motion is resulted from the interplay between these oscillations. Our findings reveal an important effect of dynamical gauge field on the nonlinear dynamics of a BEC.

1. Introduction

The emulation of gauge field in cold atomic gases is one of the major topics attracting persistent interest. Significant progress has been made in the engineering of artificial gauge field in the last decades, including both the abelian [1–4] and non-abelian gauge field, in particular, the spin–orbit coupling [4–10]. Nevertheless, most research has previously mainly focused on the realization of a static gauge field, where the generated artificial gauge field is completely determined by the external laser field, and itself has no dynamics. Recently, simulating dynamical gauge field in cold atoms has gained increasing interest and attention in the community. Until now, a variety of theoretical proposals to create dynamical gauge field have been put forward and some already been experimentally realized [11–23]. Those schemes either exploit the quantum nature of external control light, or make the gauge field dependent on the atomic density. It is an important and interesting topic to explore the new physics brought by those dynamical gauge fields [24–30].

One prominent effect induced by a static gauge field, e.g., the magnetic field, is the celebrated Hall effect for electrons in solids. For cold neutral gases, a superfluid can also exhibit Hall effect, when subject to an static artificial magnetic field [31–33]. Will the dynamical gauge field also induce a Hall effect on the transverse motion of a condensate? If true, how will the collective dynamics of the condensate be influenced by the Hall effect?

In this paper, we try to address these issues by considering dynamical gauge field which depends on the atomic density [15]. Previous studies on the effect of density-dependent gauge field mainly focus on the quasi-one-dimensional (quasi-1D) case [15, 34–36] and vortex related physics in quasi-two-dimensional (quasi-2D) case [37, 38]. To explore physics like Hall effect, the condensate dynamics has to be treated as

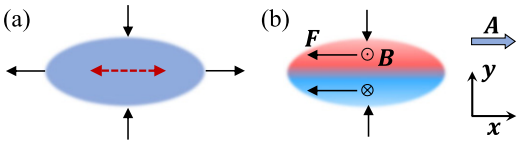

Figure 1. (a) Relevant collective modes of a BEC confined in a quasi-2D harmonic trap. The density-dependent gauge field is fixed in x direction, and couples the dipole oscillation in x direction (red dashed arrow) with breathing oscillations both in x and y directions (black arrow) (see equation (10)). The dipole oscillation in y direction is decoupled in this scenario. (b) The Hall effect induced by the density-dependent gauge field. Red and blue color denote the region where the effective magnetic field $\mathbf{B}$ points to z and $-z$ directions, respectively. The breathing oscillation in y direction can induce a dipole oscillation in x direction and vice versa, through the Lorentz force $\mathbf{F}$.

quasi-2D. In particular, we study the effect of density-dependent gauge field on the collective dynamics of a Bose–Einstein condensate (BEC) confined in a harmonic trap, beyond the linear response regime. We find that, in quasi-1D case, the dipole and breathing oscillations in the direction of gauge field are coupled, resulting in periodic or quasiperiodic motion of these modes, even when the gauge field is quite strong. While in quasi-2D case, these two modes are additionally coupled with the breathing oscillation in the perpendicular direction through the Hall effect (see figure 1), and their interplay can lead to a chaotic dynamics in the presence of a strong gauge field. Our findings shed light on the intriguing effect of dynamical gauge field on the nonlinear dynamics of BEC.

This paper is organized as follows. First, in section 2 we employ the variational wave function method to derive the coupled motion of center of mass and width, namely, the dipole mode and breathing mode of a BEC, and arrive at a set of nonlinear equations. We then solve these coupled equations numerically, with results presented in section 3, and investigate the nature of the condensate dynamics, namely, regular or chaotic. This is demonstrated by computing the Poincaré section, both in four-dimensional (4D) form and its 2D projection [39], along with the analysis of power spectrum of the dynamical variables. Finally, we end our discussion with a summary in section 4.

2. Variational wave function method

We start from the mean-field Hamiltonian which describes the atomic motion and atom–light coupling

$$\hat{H} = \left(\frac{\hat{\mathbf{p}}^2}{2m} + V(\mathbf{r})\right) \otimes \mathbb{1} + H_{\rm int} + U_{\rm AL}, \tag{1}$$

where

$$U_{\rm AL} = \frac{\hbar\Omega}{2}\begin{pmatrix} 0 & e^{-i\phi(\mathbf{r})} \\ e^{i\phi(\mathbf{r})} & 0 \end{pmatrix} \tag{2}$$

describes the coupling between two internal states $|1\rangle$ and $|2\rangle$, characterized by the two-photon Rabi frequency Ω and the laser phase $\phi(\mathbf{r})$. Here $V(\mathbf{r})$ is the external trap potential, $\mathbb{1}$ is the identity matrix defined in the pseudospin space spanned by $|1\rangle$ and $|2\rangle$, and $H_{\rm int} = (1/2)\,\mathrm{diag}\left[g_{11}\rho_1 + g_{12}\rho_2, g_{22}\rho_2 + g_{12}\rho_1\right]$ is the mean-field interaction characterized by two-body interaction strengths $g_{ll'} = 4\pi\hbar^2 a_{ll'}/m$, with $a_{ll'}$ being the scattering lengths for collisions between the components l and l'. The population of the ith state is $\rho_i = |\Psi_i|^2$ $(i = 1, 2)$.

For a dilute BEC, the coupling strength $\hbar\Omega$ is typically much larger than the mean-field energy. Therefore we can construct the interacting dressed states through perturbation theory with respect to the eigenstates of the atom–light coupling $U_{\rm AL}$, namely, diagonalizing $U_{\rm AL} + H_{\rm int}$ by treating $H_{\rm int}$ as a small perturbation. We finally obtain the eigenstates of $U_{\rm AL} + H_{\rm int}$ represented by perturbed dressed states $|\chi_\pm\rangle = |\chi_\pm^{(0)}\rangle + |\chi_\pm^{(1)}\rangle$, where

$$|\chi_\pm^{(1)}\rangle = \pm\frac{g_{11} - g_{22}}{8\hbar\Omega}\rho_\pm|\chi_\mp^{(0)}\rangle, \tag{3}$$

with eigenvalues $g\rho_\pm \pm \hbar\Omega/2$. Here $g = \left(g_{11} + g_{22} + 2g_{12}\right)/4$, $\rho_\pm = |\Psi_\pm|^2$ and the unperturbed dressed states $|\chi_\pm^{(0)}\rangle = (|1\rangle \pm \exp\{i\phi(\mathbf{r})\}|2\rangle)/\sqrt{2}$. In order to derive an interacting gauge theory, we first expand a general state as $|\xi\rangle = \sum_{i=\{+,-\}}\Psi_i(\mathbf{r}, t)\,|\chi_i\rangle$. For atomic motion slow enough, we can make the adiabatic approximation and project the general wave function into one of the two dressed states, $|\chi_\pm\rangle$. The resulting effective Hamiltonian reads

$$\hat{H}_\pm^{\rm eff} = \frac{1}{2m}(\hat{\mathbf{p}} - \mathbf{A}_\pm)^2 + V(\mathbf{r}) + W \pm \frac{1}{2}\hbar\Omega + \frac{g}{2}\rho_\pm, \tag{4}$$

where a scalar potential $W = \hbar^2|\langle\chi_-|\nabla\chi_+\rangle|^2/2m$ and a geometric vector potential $\mathbf{A}_\pm = i\hbar\langle\chi_\pm|\nabla\chi_\pm\rangle$ are introduced. According to aforementioned definition, the vector potential associated with the perturbed dressed state, to leading order, is given by

$$\mathbf{A}_\pm = \mathbf{A}^{(0)} \pm \mathbf{a}_1|\Psi_\pm(\mathbf{r})|^2. \tag{5}$$

Here $\mathbf{A}^{(0)} = -\left(\hbar/2\right)\nabla\phi(\mathbf{r})$ is the single-particle vector potential and $\mathbf{a}_1 = (\nabla\phi(\mathbf{r}))\left(g_{11} - g_{22}\right)/(8\Omega)$ controls the effective strength of density-dependent vector potential. In the following we only consider one branch of the dressed states, e.g., the + branch without loss of generality, and thus we can drop the ± index in both equations (4) and (5). Note that an effective magnetic field is associated with this density-dependent gauge field through $\mathbf{B} = \nabla\times\mathbf{A} = \nabla\rho\times\nabla\phi(\mathbf{r})\left(g_{11} - g_{22}\right)/(8\Omega)$. So the density variation of BEC results in a non-vanishing density-dependent magnetic field, which is absent in the non-interacting case for the present setup. This effective magnetic field can induce a Hall effect, as illustrated in figure 1(b), and has significant influence on the collective dynamics of BEC. We also want to emphasize that, in the simple case we consider below, both W and $\mathbf{A}^{(0)}$ are constants and can be gauged away. So, up to unimportant constants, the Hamiltonian in equation (4) is the same with $(\hat{\mathbf{p}} - \mathbf{A})^2/2m + V(\mathbf{r}) + g\rho/2$, the generic Hamiltonian accounting for the presence of gauge field $\mathbf{A}$. Additionally, the density-dependent gauge field has the most natural form $\mathbf{A}\sim\mathbf{a}_1\rho$. These two general ingredients constitute the minimal model which can simulate the condensate dynamics in the presence of density-dependent gauge field.

It was shown that BEC subject to this density-dependent gauge field obeyed a generalized Gross–Pitaevskii equation with current nonlinearity [15], and a variety of intriguing phenomena were predicted based on this equation [15, 34, 38]. Here we focus on the effect of this gauge field on the collective dynamics of BEC in a harmonic trap. Most studies on this topic usually consider a quasi-1D BEC, but as will be shown in the following, we find that the motion of a quasi-2D BEC is endowed with radically new physics. To illustrate this, we examined the dynamics of a quasi-2D BEC with motion in z direction frozen out. By using the method of variational wave function, the equation of motion is obtained by minimizing the Lagrangian

$$\mathcal{L} = \langle\Psi|\mathrm{i}\hbar\partial_t - \hat{H}^{\mathrm{eff}}|\Psi\rangle. \tag{6}$$

In particular, we choose a well-established variational wave function [40]

$$\Psi(\mathbf{r},t) = C(t)f(z)\prod_{\eta=x,y}\mathrm{e}^{-\frac{[\eta-\eta_0(t)]^2}{2w_\eta^2(t)}+\mathrm{i}\eta\alpha_\eta(t)+\mathrm{i}\eta^2\beta_\eta(t)}. \tag{7}$$

Here the harmonic potential is given by $V(\mathbf{r}) = (m\nu^2\lambda_x^2x^2 + m\nu^2\lambda_y^2y^2 + m\nu^2\lambda_z^2z^2)/2$, with the quasi-2D condition $\lambda_z \gg \lambda_i\left(i = x,y\right)$. $f(z) = \exp[-z^2/(2a_z^2)]/(\sqrt{\pi}a_z)^{1/2}$ represents the BEC wave function in z direction, with $a_z = [\hbar/(m\nu\lambda_z)]^{1/2}$ being the width of the Gaussian wave packet. The dynamical variables are the center of mass $\eta_0 = \left(x_0,y_0\right)$, amplitude $C(t)$, condensate width $w_\eta(t)$, slope $\alpha_\eta(t)$, and variables related to curvature $\beta_\eta(t)$. Plugging the variational wave function $\Psi(\mathbf{r},t)$ into equation (6) readily leads to the effective Lagrangian

$$\begin{aligned}\frac{\mathcal{L}}{N} = \sum_{\eta=x,y}\Bigg\{&\frac{\hbar}{2}\left(\dot{\beta}_\eta w_\eta^2 + 2\dot{\alpha}_\eta\eta_0 + 2\dot{\beta}_\eta\eta_0^2\right) + \frac{\hbar^2}{2m}\left[\frac{1}{2w_\eta^2} + \alpha_\eta^2 + 4\eta_0\alpha_\eta\beta_\eta + 2\left(w_\eta^2 + 2\eta_0^2\right)\beta_\eta^2\right]\\ &-\left(\frac{\hbar}{m}A_\eta^{(0)} + \frac{N\hbar a_{1\eta}}{2\sqrt{2\pi^3}ma_zw_xw_y}\right)\left(\alpha_\eta + 2\eta_0\beta_\eta\right) + \frac{1}{4}m\omega_\eta^2\left(w_\eta^2 + 2\eta_0^2\right)\Bigg\} + \frac{\tilde{g}N}{4\sqrt{2\pi^3}a_zw_xw_y}\\ &+\frac{N^2\mathbf{a}_{1\perp}^2}{6\sqrt{3}m\pi^3a_z^2w_x^2w_y^2},\end{aligned} \tag{8}$$

with $\tilde{g}/2 = g/2 + \mathbf{A}_\perp^{(0)}\cdot\mathbf{a}_{1\perp}/m$, $\mathbf{A}_\perp^{(0)} = (A_x^{(0)},A_y^{(0)})$ and $\mathbf{a}_{1\perp} = (a_{1x},a_{1y})$. The dot over the variable denotes time derivative of that variable. In terms of the notation $q_i \equiv \{w_x,w_y,x_0,y_0,\alpha_x,\alpha_y,\beta_x,\beta_y\}$, the Lagrangian equation reads

$$\frac{\mathrm{d}}{\mathrm{d}t}\left(\frac{\partial\mathcal{L}}{\partial\dot{q}_i}\right) - \frac{\partial\mathcal{L}}{\partial q_i} = 0, \tag{9}$$

from which one eventually arrives at the equations of motion of those dynamical variables.

For computational simplicity and without loss of generality, we assume the laser phase takes the form of a plane wave along x direction, namely, $\phi(\mathbf{r}) = kx$. Thus, the density-dependent gauge field is also along x direction. After introducing dimensionless variables and constants according to $\tau = \nu t$, $R_\eta = w_\eta/l_0$

$(\eta = x, y)$, $R_z = a_z/l_0$, $P_x = k(g_{11} - g_{22})N/(8\hbar\Omega l_0^2)$, $P_y = 0$, and $G = gN/\left(\hbar\nu l_0^3\right)$, where $l_0 = \left[\hbar/\left(m\nu\right)\right]^{1/2}$, the resulting equations of motion finally read as follows:

$$\begin{aligned}
\frac{\mathrm{d}^2\eta_0}{\mathrm{d}\tau^2} + \lambda_\eta^2\eta_0 &= \frac{P_\eta}{2\sqrt{2\pi^3}R_zR_xR_y}\sum_{\xi=x,y}\frac{1}{R_\xi}\frac{\mathrm{d}R_\xi}{\mathrm{d}\tau},\\
\frac{\mathrm{d}^2R_\eta}{\mathrm{d}\tau^2} + \lambda_\eta^2R_\eta &= \frac{1}{R_\eta^3} + \left(\frac{2}{3\sqrt{3}} - \frac{1}{4}\right)\frac{P_x^2}{\pi^3R_z^2R_\eta R_x^2R_y^2}\\
&\quad + \left(\frac{1}{2}G - P_x\frac{\mathrm{d}x_0}{\mathrm{d}\tau}\right)\frac{1}{\sqrt{2\pi^3}R_zR_\eta R_xR_y}.
\end{aligned} \tag{10}$$

Note that since the density-dependent gauge field has been fixed in x direction, the center of mass motion in y direction becomes decoupled, and the strength of the density-dependent gauge field is characterized by the dimensionless constant P_x.

In the absence of density-dependent gauge field, these equations describe the dipole and breathing modes of BEC [40], respectively. The dipole and breathing oscillations in x direction are always coupled, and for quasi-1D case, these are the only two relevant modes. For quasi-2D case, the gauge field also introduces a nontrivial coupling between the dipole mode in x direction and the breathing mode in y direction, reminiscent of the Hall effect induced by the gauge field (figure 1), which is crucial for a comprehensive description of the condensate dynamics. This coupling shows the key distinction between quasi-2D and quasi-1D cases, and plays an important role in the emergence of chaotic dynamics in quasi-2D case.

3. Chaotic dynamics

Before solving the coupled nonlinear equations, we first note that the original Hamiltonian does not change with time, so the total energy is conserved,

$$\begin{aligned}
\frac{E}{N} &= \frac{1}{4}\sum_{\eta=x,y}\left[\frac{1}{R_\eta^2} + \dot{R}_\eta^2 + 2\dot{\eta}_0^2 + \lambda_\eta^2\left(R_\eta^2 + 2\eta_0^2\right)\right]\\
&\quad + \frac{G}{4\sqrt{2\pi^3}R_zR_xR_y} + \frac{1}{4}\left(\frac{2}{3\sqrt{3}} - \frac{1}{4}\right)\frac{P_x^2}{\pi^3R_z^2R_x^2R_y^2},
\end{aligned} \tag{11}$$

where an unimportant constant $W + \hbar\Omega/2$ is dropped out. Due to the conservation of total energy, when computing the Poincaré sections in the following, the total energy serves as a constrain for reducing the dimension of phase space. In addition, we first calculate the lowest energy $E_{\min}$ at given parameters, and then use it as the energy unit.

For small amplitude oscillation, i.e., in the linear response regime, these equations can be linearized to give the frequency of coupled motion. To study oscillations of larger amplitude, or higher energy modes, one has to numerically solve these coupled equations to obtain the center of mass motion, along with the width motion of the condensate. The density-dependent gauge field couples these two kinds of motion, making the overall dynamics complicated. Here the spatial dimension of the underlying dynamics is crucial.

For comparison, we first consider the quasi-1D case. The condensate is tightly confined both in y and z directions, with their widths fixed to be the same $R_y = R_z$. The dynamical variables are then x_0, $\dot{x}_0$, R_x and $\dot{R}_x$. As the dimension of the phase space is four, by fixing the total energy as well as another dynamical variable, e.g., $\dot{R}_x = 0$, we obtain a conventional 2D Poincaré section in the x_0–$\dot{x}_0$ plane. The Poincaré section for two typical strengths of density-dependent gauge field is shown in figure 2. One sees that whether the density-dependent gauge field is weak (figure 2(a)) or strong (figure 2(b)), there are only regular dots and closed curves in the Poincaré section. These regular dots and closed curves correspond to periodic and quasiperiodic orbits, respectively. The quasiperiodic motion may result from the irrational frequency ratio of dipole mode over breathing mode.

For the quasi-2D case, as the center of mass motion in y direction is decoupled, the remaining relevant dynamical variables are x_0, $\dot{x}_0$, R_x, $\dot{R}_x$, R_y and $\dot{R}_y$. The phase space is six-dimensional, and thus by fixing the total energy along with $\dot{R}_x = 0$, the Poincaré section is 4D. In principle, one can also add two other constrains, e.g., by additionally fixing both R_x and R_y, to obtain a 2D Poincaré section, which however proves to be numerically quite challenging because of sparsity of those intersection points. In the present study, we use a 2D projection to illustrate the overall feature of the 4D Poincaré section, in conjunction with

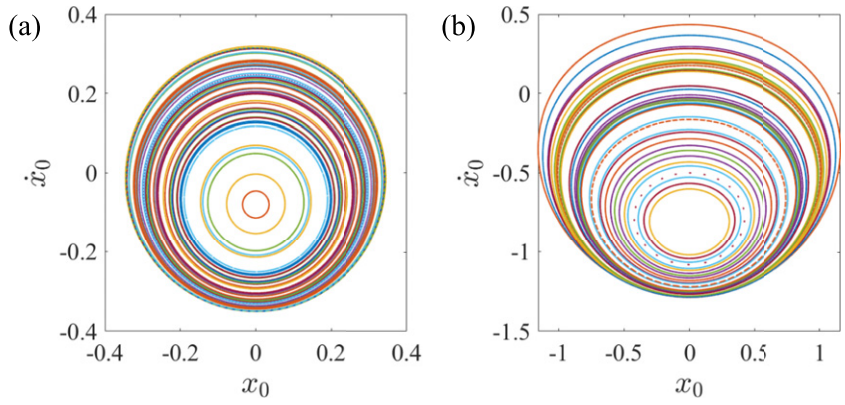

Figure 2. 2D Poincaré section of quasi-1D center of mass motion. Different color denotes different initial conditions. (a) $P_x = 0.5$, $E = 1.02^* E_{\min}$. (b) $P_x = 3$, $E = 1.2^* E_{\min}$. The other parameters are $R_y = 0.2$, $R_z = 0.2$, $\lambda_x = 1$, and $G = 5$.

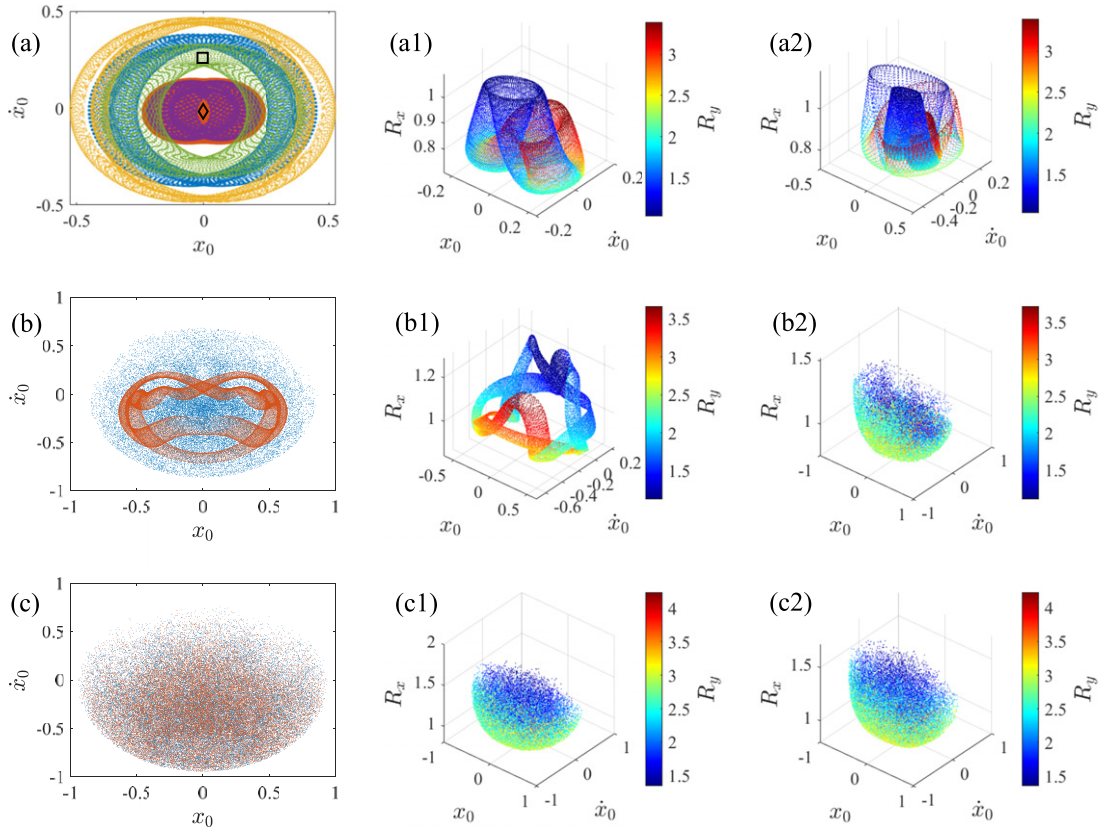

Figure 3. Projected 2D Poincaré section on the x_0–$\dot{x}_0$ plane and 4D Poincaré section for certain orbits. (a) For weak density-dependent gauge field, only quasiperiodic orbits are present in Poincaré section. Different colors represent orbits with different initial conditions. The original 4D orbits for the central dark red curve (with diamond marker) and outer green curve (with square marker) are shown in (a1) and (a2), respectively. $P_x = 0.2$. (b) For moderate strength of gauge field, the phase space consists of quasiperiodic (dark red) and chaotic (dark blue) orbits, with their 4D form shown in (b1) and (b2), respectively. $P_x = 4$. (c) For strong gauge field, the Poincaré section consists of a chaotic sea, with scattered dark red and dark blue dots representing two chaotic orbits in (c1) and (c2) with different initial conditions. $P_x = 10$. The other parameters are $R_z = 0.2$, $\lambda_x = 1$, $\lambda_y = 0.5$, $G = 5$, and $E = 1.3^* E_{\min}$.

4D visualization of certain orbits, similar to methods previously introduced elsewhere [39]. The 2D projection is on the x_0–$\dot{x}_0$ plane, and the 4D visualization of certain orbits is achieved via a three-dimensional plot of x_0, $\dot{x}_0$, and R_x, with R_y represented by color.

Figure 3 shows the Poincaré section using the method described above, including its original 4D form and 2D projection on the x_0–$\dot{x}_0$ plane. Only limited number of initial conditions are chosen in computing the Poincaré section, as those curves in projected 2D Poincaré section can overlap with each other, messing the Poincaré section for large number of initial conditions. This feature is in stark contrast with

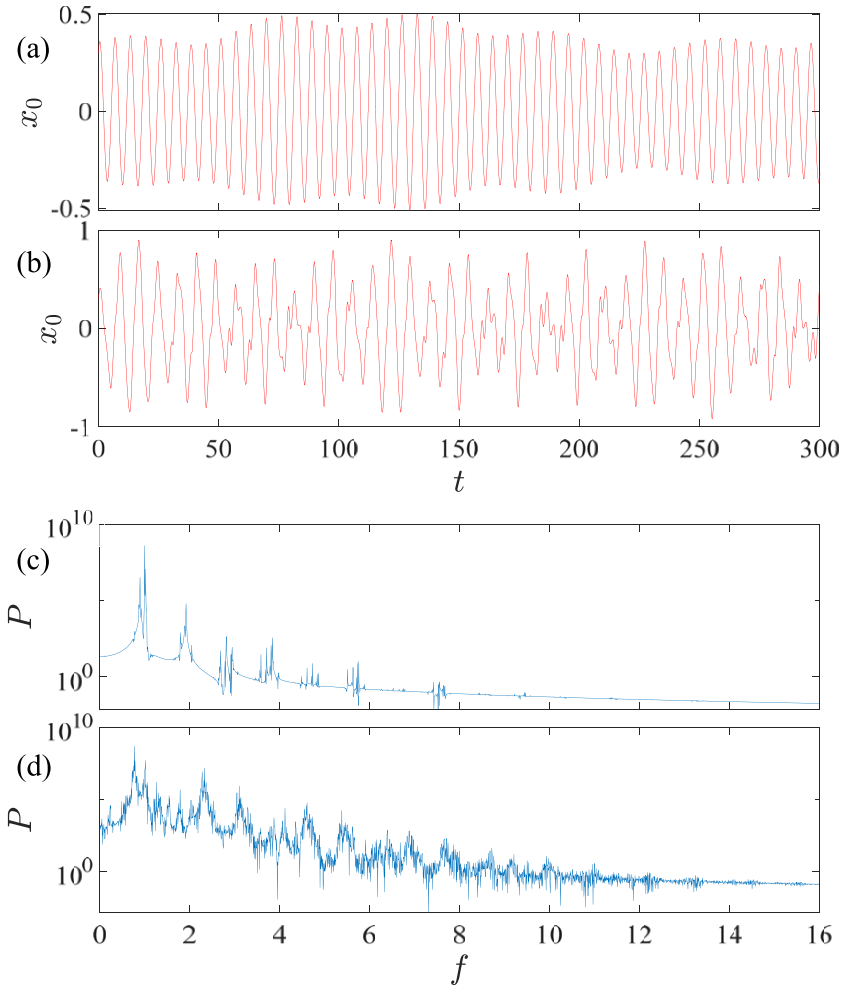

Figure 4. Quasiperiodic and chaotic dynamics of center of mass motion shown in time domain ((a) and (b)) and their power spectrums ((c) and (d)) in quasi-2D case. (a) and (c) show the quasiperiodic motion, with $P_x = 0.2$. (b) and (d) show the chaotic motion, with $P_x = 10$. Time t is in the unit of $1/\nu$ and frequency f is in the unit of ν. The other parameters are $R_z = 0.2$, $\lambda_x = 1$, $\lambda_y = 0.5$, $G = 5$, and $E = 1.3^* E_{\min}$.

conventional 2D Poincaré section, where regular and chaotic orbits do not overlap with each other. When the density-dependent gauge field is weak, the projected 2D Poincaré section (figure 3(a)) consists of various distorted closed curves, which are originally distorted tori in the 4D Poincaré section (figures 3(a1) and (a2)). So we conclude that these closed curves in projected 2D Poincaré section correspond to quasiperiodic orbits. Figures 3(a1) and (a2) show the original 4D Poincaré section for two different initial conditions, corresponding to the central dark red (with diamond marker) and outer green curves (with square marker) in figure 3(a), respectively. With the increase of the strength of gauge field, chaotic orbits eventually appears, as shown by the scattered points in the chaotic sea of figure 3(b2), and its 2D projection in figure 3(b) (dark blue dots). Note that once the center of mass motion becomes chaotic, the motion of widths R_x and R_y are also chaotic. So one can also choose to project the 4D Poincaré on other 2D planes, and similar 2D chaotic sea will be observed. In this parameter regime, the Poincaré section consists of coexisting quasiperiodic (see figure 3(b1), corresponding to dark red dots in figure 3(b)) and chaotic orbits.

For sufficiently strong density-dependent gauge field, e.g., in the parameter regime shown in figure 3(c), we only find chaotic orbits starting from various initial conditions. Figures 3(c1) and (c2) show the chaotic orbits with two different initial conditions in the 4D Poincaré section, with figure 3(c) being their 2D projections. The whole phase space in the Poincaré section is occupied by chaotic orbits. We also vary the strength of gauge field, total energy and trap anisotropy, and results show that stronger gauge field, higher energy and stronger trap anisotropy all favor the appearance of chaos in the collective motion of BEC.

To further confirm the nature of these chaotic orbits, we choose a typical initial condition in the chaotic sea of figure 3(c), and show the time evolution as well as the power spectrum of one typical chaotic orbit in figures 4(b) and (d). Here the power spectrum is defined as $P_f = |q_f|^2$, with q_f being the Fourier transform

of time dependent variable q at frequency f. The chaotic dynamics is manifested by the broad and structureless feature in power spectrum. For comparison, the time evolution and power spectrum of a typical quasiperiodic orbit is also shown in figures 4(a) and (c), with same parameters as figure 3(a). The distinction between these two kinds of orbits is clear in both time evolution and power spectrum, consistent with our judgment based on Poincaré section.

The chaotic dynamics can be qualitatively understood as the interplay between three oscillations, namely, the dipole and breathing oscillations along the direction of gauge field, and the breathing oscillation in perpendicular direction (figure 1(a)). The former two modes are coupled through the current nonlinearity [15], while the dipole and breathing modes in perpendicular directions are coupled by the interaction induced Hall effect (figure 1(b)), only present for system of dimension two or higher. This explains the dramatic difference between quasi-1D and quasi-2D dynamics.

There are in fact various proposals for generating different forms of density-dependent gauge field. For example, in reference [23], the authors experimentally realized a gauge field that takes one of two values, and observed the 1D dynamics of domain wall driven by synthetic electric field. The transverse motion of condensate induced by synthetic magnetic field as studied here will be an interesting subject for future experimental exploration. On the other hand, our calculations are based on another proposal [15], which can realize a general form of density-dependent gauge field $\mathbf{A} \sim \mathbf{a}_1\rho$. According to this proposal, below we give an estimate of the maximum strength of gauge field, namely, P_x. For clarity, we first factorize it into three factors $P_x = \frac{(g_{11}-g_{22})\bar{\rho}}{8\hbar\Omega} \times \frac{N}{4\pi\bar{\rho}l_z l_0^2/3} \times \frac{8\pi^2 l_z}{3\lambda}$. Here $\bar{\rho}$ is the average condensate density, λ is the optical wavelength and l_z is the harmonic oscillator length in z direction. Each factor is dimensionless and has its own range of tunability. The first factor is related with the validity of perturbation theory (see equation (3)), and thus its maximum value is ~ 0.2. For typical scattering lengths difference ~ 5 nm tunable by Feshbach resonance [41], average condensate density $\sim 10^{15}$ cm^{-3}, and Rabi frequency ~ 10 kHz, this maximum value can be reached. The second factor is the order of 1. The third factor can also be tuned. For example, choosing harmonic oscillator length $l_z \sim 1.2$ μm and optical wavelength ~ 600 nm, this factor is ~ 50. So the overall value of P_x can reach 10, within the parameter regime of our calculations. Once a density-dependent gauge field of the natural form $\mathbf{A} \sim \mathbf{a}_1\rho$ is experimentally realized, further demonstration of the novel physics predicted here only involves standard experimental techniques. Different initial states with desired center of mass or condensate width can be prepared by first loading a BEC into the ground state of a harmonic trap, and then quenching the trap center or trap frequency, respectively. The chaotic dynamics of BEC will be observed by measuring either the center of mass or the width motion of BEC in a harmonic trap.

4. Conclusion

In summary, we have studied the effect of density-dependent gauge field on the collective dynamics of a harmonically trapped BEC. The nature of the collective dynamics depends sensitively on the spatial dimension of the condensate. For a quasi-1D BEC, we only find periodic and quasiperiodic motions, whether the gauge field is weak or strong. In contrast, for a quasi-2D BEC and strong gauge field, we find that the center of mass motion can become chaotic. This is also true for the dynamics of condensate width. The chaotic behavior is induced by the interplay between the dipole oscillation in the direction of gauge field and the breathing oscillations both along and perpendicular to that direction. The coupling between dipole and breathing oscillations in perpendicular direction can be understood as a Hall effect induced by the gauge field. We confirm the chaotic dynamics by computing the 4D Poincaré section, its projection on 2D plane, and the power spectrum. We find strong density-dependent gauge field, trap anisotropy and high energy are favorable for the observation of chaotic dynamics. Our findings deepen our understanding of the effect of dynamical gauge field in cold atomic gases, especially on the nonlinear dynamics of BEC.

Acknowledgments

We thank Qiong-Tao Xie and Biao Wu for helpful discussions. LC is supported by the Science Foundation of Guizhou Science and Technology Department (Grant Nos. QKHJZ[2021]033 and QKHJZ[2018]1178), and the Science Foundation of Guizhou Provincial Education Department (Grant No. QJHKYZ[2017]087). QZ is supported by the National Natural Science Foundation of China (Grant No. 12004118), the Guangdong Basic and Applied Basic Research Foundation (Grant No. 2020A1515110228 and 2021A1515010212), and the Science and Technology Program of Guangzhou (Grant No. 2019050001).

Data availability statement

The data that support the findings of this study are available upon reasonable request from the authors.

ORCID iDs

Qizhong Zhu https://orcid.org/0000-0002-9798-9075

References

[1] Lin Y-J, Compton R L, Jiménez-García K, Porto J V and Spielman I B 2009 *Nature* **462** 628
[2] Lin Y-J, Compton R L, Jiménez-García K, Phillips W D, Porto J V and Spielman I B 2011 *Nat. Phys.* **7** 531
[3] Dalibard J, Gerbier F, Juzeliūnas G and Öhberg P 2011 *Rev. Mod. Phys.* **83** 1523
[4] Goldman N, Juzeliūnas G, Öhberg P and Spielman I B 2014 *Rep. Prog. Phys.* **77** 126401
[5] Lin Y-J, Jiménez-García K and Spielman I B 2011 *Nature* **471** 83
[6] Wang P, Yu Z-Q, Fu Z, Miao J, Huang L, Chai S, Zhai H and Zhang J 2012 *Phys. Rev. Lett.* **109** 095301
[7] Cheuk L W, Sommer A T, Hadzibabic Z, Yefsah T, Bakr W S and Zwierlein M W 2012 *Phys. Rev. Lett.* **109** 095302
[8] Zhai H 2015 *Rep. Prog. Phys.* **78** 026001
[9] Huang L, Meng Z, Wang P, Peng P, Zhang S-L, Chen L, Li D, Zhou Q and Zhang J 2016 *Nat. Phys.* **12** 540
[10] Wu Z *et al* 2016 *Science* **354** 83
[11] Keilmann T, Lanzmich S, McCulloch I and Roncaglia M 2011 *Nat. Commun.* **2** 361
[12] Banerjee D, Dalmonte M, Müller M, Rico E, Stebler P, Wiese U-J and Zoller P 2012 *Phys. Rev. Lett.* **109** 175302
[13] Zohar E, Cirac J I and Reznik B 2013 *Phys. Rev. Lett.* **110** 125304
[14] Tagliacozzo L, Celi A, Orland P, Mitchell M W and Lewenstein M 2013 *Nat. Commun.* **4** 2615
[15] Edmonds M J, Valiente M, Juzeliūnas G, Santos L and Öhberg P 2013 *Phys. Rev. Lett.* **110** 085301
[16] Greschner S, Sun G, Poletti D and Santos L 2014 *Phys. Rev. Lett.* **113** 215303
[17] Ballantine K E, Lev B L and Keeling J 2017 *Phys. Rev. Lett.* **118** 045302
[18] Clark L W, Anderson B M, Feng L, Gaj A, Levin K and Chin C 2018 *Phys. Rev. Lett.* **121** 030402
[19] Schweizer C, Grusdt F, Berngruber M, Barbiero L, Demler E, Goldman N, Bloch I and Aidelsburger M 2019 *Nat. Phys.* **15** 1168
[20] Görg F, Sandholzer K, Minguzzi J, Desbuquois R, Messer M and Esslinger T 2019 *Nat. Phys.* **15** 1161
[21] Kroeze R M, Guo Y and Lev B L 2019 *Phys. Rev. Lett.* **123** 160404
[22] Xu P, Deng T-S, Zheng W and Zhai H 2021 *Phys. Rev.* A **103** L061302
[23] Yao K-X, Zhang Z and Chin C 2022 *Nature* **602** 68
[24] Dong L, Zhou L, Wu B, Ramachandhran B and Pu H 2014 *Phys. Rev.* A **89** 011602
[25] Zheng J-h, Xiong B, Juzeliūnas G and Wang D-W 2015 *Phys. Rev.* A **92** 013604
[26] Raventós D, Graß T, Juliá-Díaz B, Santos L and Lewenstein M 2016 *Phys. Rev.* A **93** 033605
[27] Zheng W and Cooper N R 2016 *Phys. Rev. Lett.* **117** 175302
[28] Yao Z, Liu C, Zhang P and Zhai H 2020 *Phys. Rev.* B **102** 104302
[29] Valentí-Rojas G, Westerberg N and Öhberg P 2020 *Phys. Rev. Res.* **2** 033453
[30] Kirichenko E V, Stephanovich V A and Sherman E Y 2020 *Ann. Phys.* **532** 2000012
[31] Zhu S-L, Fu H, Wu C-J, Zhang S-C and Duan L-M 2006 *Phys. Rev. Lett.* **97** 240401
[32] LeBlanc L J, Jiménez-García K, Williams R A, Beeler M C, Perry A R, Phillips W D and Spielman I B 2012 *Proc. Natl Acad. Sci. USA* **109** 10811
[33] Choi J-y, Kang S, Seo S W, Kwon W J and Shin Y-i 2013 *Phys. Rev. Lett.* **111** 245301
[34] Edmonds M J, Valiente M and Öhberg P 2015 *Europhys. Lett.* **110** 36004
[35] Dingwall R J, Edmonds M J, Helm J L, Malomed B A and Öhberg P 2018 *New J. Phys.* **20** 043004
[36] Dingwall R J and Öhberg P 2019 *Phys. Rev.* A **99** 023609
[37] Butera S, Valiente M and Öhberg P 2016 *New J. Phys.* **18** 085001
[38] Edmonds M and Nitta M 2020 *Phys. Rev.* A **102** 011303
[39] Lukes-Gerakopoulos G, Katsanikas M, Patsis P A and Seyrich J 2016 *Phys. Rev.* D **94** 024024
[40] Pérez-García V M, Michinel H, Cirac J I, Lewenstein M and Zoller P 1996 *Phys. Rev. Lett.* **77** 5320
[41] Chin C, Grimm R, Julienne P and Tiesinga E 2010 *Rev. Mod. Phys.* **82** 1225